Inorganic Chemistry

Article

pubs.acs.org/IC

Computational Examination on the Active Site Structure of a (Peroxo)diiron(III) Intermediate in the Amine Oxygenase AurF

Prabha Jayapal,* Azaj Ansari, and Gopalan Rajaraman*

Department of Chemistry, Indian Institute of Technology Bombay, Mumbai 400076, India

Supporting Information

ABSTRACT: In this work, we report the first computational investigation on the structure and properties of the (peroxo)diiron(III) intermediate of the AurF enzyme. Our calculations predict that, in the oxidized state of the AurF enzyme, the peroxo ligand is depicted in a μ-1,1-coordination mode with a protonated bridging ligand and is not in a μ-η^2:η^2 or μ-1,2 mode. Computed spectral data for the μ-1,1-coordination mode correlate well with experimental observations and unravel the potential of the energetics−spectroscopic approach adapted here.

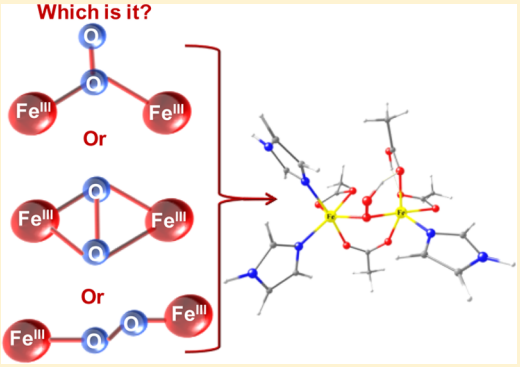

INTRODUCTION

p-Aminobenzoate *N*-oxygenase (AurF) from *Streptomyces thioluteus* is a diiron enzyme[1] that catalyzes the conversion of *p*-aminobenzoate to *p*-nitrobenzoate ($ArNO_2$) in the biosynthesis of the antibiotic aureothin[1,2] and has structural similarity with other dinuclear metalloenzymes.[3] The X-ray crystal structure of AurF has been independently solved by two groups claiming Fe−Fe[4] and Mn−Mn[2] compositions. Choi et al.[4] have reported in vitro reconstitution of the AurF enzyme activity and crystal structure of the AurF enzyme in the oxidized state. From this crystal structure, it has been identified that the active site of AurF comprises a Fe_2 center bridged by a μ-O group. It has also been proposed that the residues Glu-101, Glu-136, His-139, Glu-196, His- 223, Glu-227, and His-230 engage these two Fe sites (see Figure 1). Our earlier calculations fully support these assignments.[5] The Mössbauer (MB) and UV−vis spectroscopic[4b,6] data propose that, during the mechanistic cycle, the native enzyme generates various intermediates to catalyze the reaction. Also, a long-lived peroxodiiron(III) species has been trapped after the addition of O_2 to the resting state of the enzyme,[4b,6] and this peroxodiiron(III) species initiates the catalytic cycle. However, the catalytic mechanism remains unclear because of the lack of the crystal structure of the intermediates involved in the reaction. Besides, the peroxo intermediate of AurF may possess three different coordination modes, such as μ-η^2:η^2, μ-1,1, or μ-1,2, and all three modes have been identified in other diiron enzymes, such as methane monooxygenase (MMO),[3e,f] soluble Δ9 desaturase,[3g] and ribonucleotide reductase (RNR).[3h] On the basis of the stopped-flow absorption measurements and MB observations, Li et al.[6] have suggested that the oxygenated species could be a peroxo or hydroperoxo species in a μ-1,1 or distorted μ-η^2:η^2 mode but ruled out the possibility of the μ-1,2 mode. Despite these studies, the exact structure and properties of the oxygen adduct of this enzyme are still unclear.

Nowadays, quantum-chemical methods are widely used to determine the electronic structures of the metalloenzymes, and they offer significant insight into the system with respect to the structure, energies, and spectral properties.[3c,7,8] Using computational methods, here we aim to address the following issues: (1) What is the ground-state structure of the oxygenated form of the diiron AurF? (2) Are peroxo/carboxylate groups protonated in the native state of the enzyme? This has relevance to the observed spectral features and its reactivity toward organic substrates. (3) Can theoretical spectroscopy (computing MB and UV−vis data) be used to unequivocally assign the ground-state structure?

COMPUTATIONAL METHODOLOGY

The popular B3LYP-D2 functional[9] in conjunction with the TZVP[10] basis set for Fe and the SVP[10] basis set for the rest of the elements is used for optimization. Frequency calculations are performed on the optimized structures to verify that they are minima on the potential energy surface. Besides, the solvent effects are incorporated using the polarizable continuum model, employing water as the solvent. Thus, the quoted energies are the B3LYP-D2 functional computed solvent-free energies, unless otherwise mentioned. All initial coordinates are obtained from the X-ray crystal structure of the oxidized AurF enzyme[4a] (PDB code: 3CHU) and modeled according to the coordination mode. An unrestricted density functional theory (UDFT) methodology is used to model the spin polarization efficiently for open-shell orbitals of both Fe atoms. This method enables modeling of antiferromagnetic (AF) coupling between the two Fe atoms by the use of a broken-symmetry (BS) wave function.

Received: April 17, 2015
Published: November 20, 2015

DOI: 10.1021/acs.inorgchem.5b00872
Inorg. Chem. 2015, 54, 11077−11082

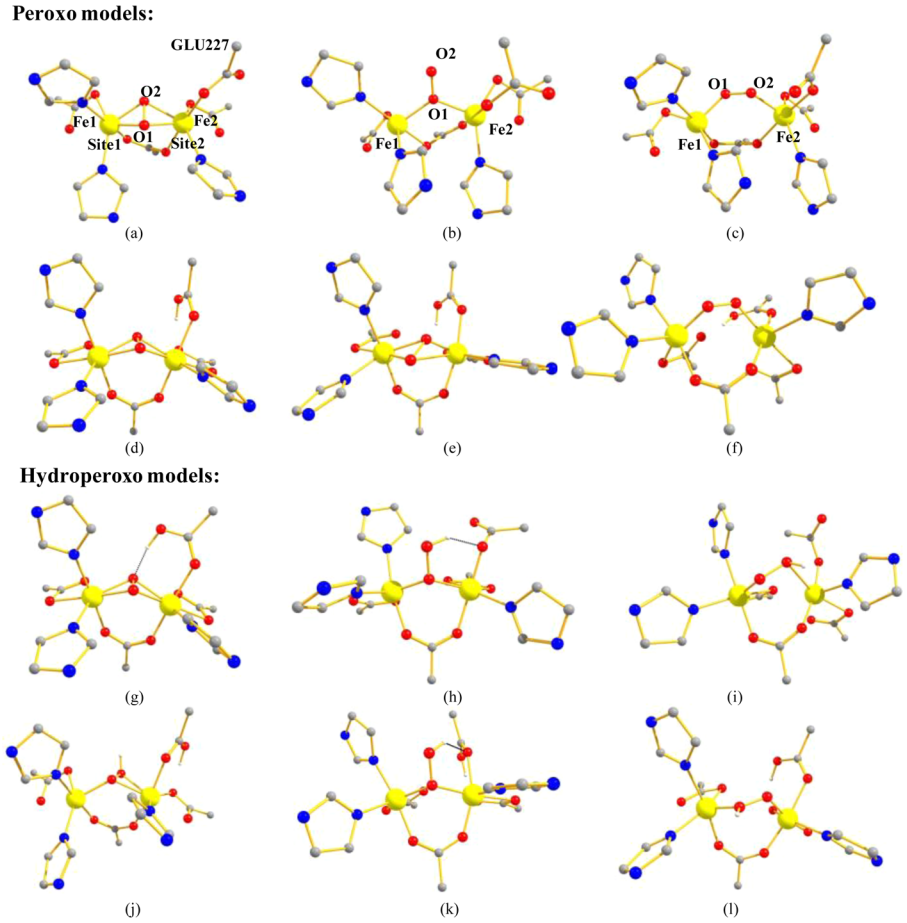

Figure 1. B3LYP-D2-optimized geometries of the quantum-chemical cluster models (a) M1, μ-η^2:η^2-peroxodiiron(III/III), (b) M2, μ-1,1-peroxodiiron(III/III), (c) M3, μ-1,2- peroxodiiron(III/III) complexes along with the possible peroxodiiron(III) models (d) $_{227}$M1, (e) $_{227}$M2, and (f) $_{227}$M3, where the Fe−Fe distances are 3.483, 3.702, 4.023, 3.482, 3.410, and 3.568 Å, respectively. For the hydroperoxodiiron(III) models, (g) M1P, μ-η^2:η^2-hydroperoxodiiron(III/III), (h) M2P, μ-1,1-hydroperoxodiiron(III/III), and (i) M3P, μ-1,2-hydroperoxodiiron(III/III) models along with GLU227-protonated (j) $_{227}$M1P, (k) $_{227}$M2P, and (l) $_{227}$M3P, where the Fe−Fe distances are 3.532,3.463, 3.670, 3.707, 3.488, and 3.894 Å, respectively. Refer to Tables S1 and S2 for complete bond distance information. Only H atoms involved in hydrogen-bonding interactions are shown, and others are removed for clarity.

Geometry optimization is carried out with *Gaussian 09* software,[11] whereas all spectroscopic parameters are calculated with the *ORCA 2.8* program package.[12] The best functional has been chosen based on the property of interest as reported earlier.[13,14] Because the prediction of these parameters requires a reasonable estimation of the spin densities on the metal centers, the employed functional plays a crucial role in computing these parameters. The MB parameters are calculated using the BP86[9b,15] functional and TZVP basis set. However, the UV spectral calculations and Heisenberg coupling constants J are obtained by employing the B3LYP functional and TZVP basis set. All spectroscopic calculations also incorporate the solvent effect, employing water as a solvent. The MB isomer shifts δ are calculated based on $\rho(0)$ using the following equation:

$$\delta = \alpha[\rho(0) - A] + C \quad (1)$$

where A and C are constants and $\rho(0)$ is the electron density at the nucleus.

The magnetic exchange interaction has been computed using the following spin Hamiltonian:

$$\hat{H} = -J\hat{S}_{Fe1}\hat{S}_{Fe2} \quad (2)$$

Here J is the exchange coupling constant and S_{Fe1} and S_{Fe2} are spin values on the individual Fe^{III} centers ($S = {}^5/_2$ here). The magnetic exchange has been computed as the difference in energy between the high-spin and BS states, as proposed by Noodleman.[16] Many equations have been (spin-projected and non-spin-projected)[17] advocated to compute the J values, and here we employ the methodology advocated by Ruiz and co-workers,[17] which has been shown to provide a good numerical estimate of the J values for several systems. Besides, for systems that exhibit significant radical behavior on the O atom, three different exchange parameters are employed to extract the J values. The following Hamiltonian is used in such cases:

$$H = -J_1\hat{S}_{Fe1}\hat{S}_{Fe2} - J_2\hat{S}_{Fe1}\hat{S}_{O1} - J_3\hat{S}_{O1}\hat{S}_{Fe2} \quad (3)$$

Here Fe1, Fe2, and O1 represent spins on the Fe1, Fe2, and O1 centers. Here four spin configurations are employed to compute three different exchange interactions.[18] All of the energies quoted here are B3LYP-D2 energies incorporating free-energy corrections at 298.15 K.

RESULTS

In this contribution, we report the first theoretical investigation to probe the structure of the oxygen adduct of the AurF enzyme by computing the geometries, electronic structures, energetics, and, most importantly, spectroscopic parameters of different peroxo and hydroperxo models (see Figure 1) to shed light on the ground-state structure of the peroxodiiron(III) oxidized species. Six sets of model complexes having the core structure of $\{Fe_2^{III}OO\}$ with (i) μ-η^2:η^2 coordination (butterfly structure; termed as model M1) (ii) μ-1,1 coordination (M2), and (iii) μ-1,2 coordination (M3) modes along with their μ-

DOI: 10.1021/acs.inorgchem.5b00872
Inorg. Chem. 2015, 54, 11077−11082

Table 1. Calculated and Experimental[4b] Isomer Shift δ (mm/s), Quadrupole Splitting ΔE_q (mm/s) Parameters, B3LYP-D2-Computed Relative Energies (kJ/mol), Net Spin Population (NSP), and Heisenberg Coupling Constant J (cm^{-1}) of Peroxodiiron(III) and Hydroperoxodiiron(III) Model Complexes Investigated

	NSP				spectroscopic parameters: Δ		ΔE_q			
species	Fe1	Fe2	μ-O1	μ-O2	Fe1	Fe2	Fe1	Fe2	relative energy (ΔG)	J (cm^{-1})
Peroxodiiron(III/III) Model Complexes										
M1	4.15	−4.15	−0.02	−0.05	0.74	0.73	−0.59	−0.59	465.6	−123.5
M2	4.19	−3.80	−0.22	−0.58	0.68	0.69	0.87	−0.65	419.4	−97.8 (−4.6, −119.5, −365.5)[a]
M3	4.13	−4.08	−0.34	0.18	0.70	0.65	0.72	1.23	477.9	−136.4
$_{227}$M1	4.14	−4.16	0.04	0.01	0.75	0.70	0.92	−0.69	37.2	−142.9
$_{227}$M2	4.20	−4.22	−0.09	0.00	0.66	0.70	1.22	−0.95	43.6	−172.5
$_{227}$M3	4.14	−4.08	−0.34	0.20	0.67	0.67	1.32	1.16	43.0	−158.2
Exp[4b]	NA	NA	NA	NA	0.54	0.61	−0.66	0.35	NA	NA
Hydroperoxodiiron(III/III) Model Complexes										
M1P	4.16	−4.18	0.01	0.00	0.73	0.70	1.033	−0.63	37.0	−113.8
M2P	4.00	−4.04	0.00	0.00	0.61	0.58	−0.55	−0.68	84.4	−61.7
M3P	4.18	−4.15	−0.35	−0.02	0.71	0.58	0.81	1.06	119.9	−40.6
$_{227}$M1P	4.19	−4.22	−0.01	0.05	0.71	0.55	−0.80	0.59	27.9	−75.3
$_{227}$M2P	4.22	−4.23	−0.04	−0.01	0.65	0.57	−0.78	0.78	0.0	−68.4
$_{227}$M3P	4.21	−4.23	−0.04	0.20	0.63	0.56	1.06	0.76	35.9	−30.3

[a]Here two types of calculations are performed, assuming only the Fe−Fe interaction, and modeled with one J, assuming three different interactions between Fe and the radical centers. These J values are given in parentheses (see Figure 2 and the corresponding text for details).

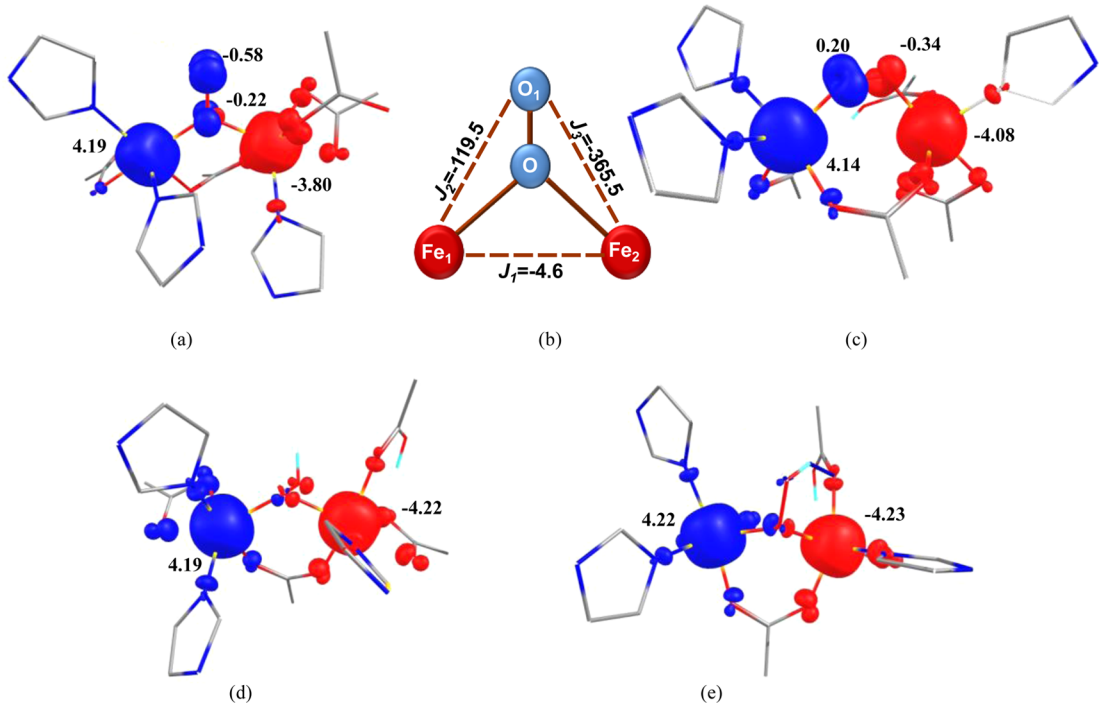

Figure 2. B3LYP-D2-computed (a) spin density plot of M2 and (b) adapted magnetic exchange scheme for the M2 model. Spin density plots of (c) $_{227}$M3, d) $_{227}$M1P, and e) $_{227}$M2P models.

OOH protonated counterparts (denoted as M1P, M2P, and M3P models) have been modeled. We have also attempted to establish the protonation state of the terminal glutamate (GLU227 as per ref 4a) at site 2 by expanding the test set to 12 models (see Figure 1).[19]

B3LYP-D2[8c]-optimized selected structural parameters of the computed models in comparison to the X-ray structure are given in Figure 1 (see also Figure S1 and Tables S1 and S2). It is important to note here that the X-ray structure reported is for the diferric form and has been given here only to draw general structural attributes. The peroxo models M1, $_{227}$M1, and M2 with either μ-η^2:η^2 or μ-1,1 mode have the Fe−Fe, Fe−O, and O−O distances comparable with the DFT-computed values for other dinuclear Fe enzymes possessing the same coordination mode.[3h,20] From the Fe−O1−O2−Fe dihedral angle (Figure 1 and Table S1), we understood that the type of constraint provided by the additional O2 bridge in M1 is not present in M2. Hence, the distal O atom of the peroxo ligand in M2 can easily form a hydrogen bond with the terminal histidine ligand of the Fe1 center (site 1). This offers an explanation for the

DOI: 10.1021/acs.inorgchem.5b00872
Inorg. Chem. 2015, 54, 11077−11082

presence of additional histidine ligands in the AurF enzyme compared to other enzymes possessing a similar structural motif at the active site.[3,20] The optimized geometry of M3 resembles a *cis*-μ-1,2-peroxo model of RNR[3h] with Fe1−Fe2, Fe1−O1, and Fe2−O2 bond lengths of 4.023, 1.855, and 1.920 Å, respectively. The increased Fe−Fe bond distance of the M3 models in comparison to the M1 models is due to the transformation of bridging O2 from the side-on to the end-on mode. Except in the $_{227}$M1P model, in all other studied hydroperoxo models, the peroxo unit is in hydrogen-bonding interaction with the neighboring terminal glutamate unit. This is important for the proper geometrical positioning of the ligands similar to the earlier reported dinuclear active site structure,[21,22] where protonation of the O_2^{2-} group is suggested as the first step in the catalytic activation.[23]

Computed energies suggest the $_{227}$M2P model with μ-1,1-hydroperoxodiiron(III/III) coordination mode, with the terminal glutamate being protonated as the ground state (see Table 1). This is followed by the M1P model possessing μ-η^2:η^2 butterfly structure (37 kJ/mol). It was observed that the glutamate-protonated hydroperoxo models (M2P and M3P) are nearly 5 times lower in energy compared to its unprotonated counterparts (M2 and M3; Table 1). We can also infer that the energy difference between the energetically most stable hydroperoxo $_{227}$M2P model and its peroxo counterpart $_{227}$M2 is ∼43 kJ/mol. This energy difference between the protonated and nonprotonated models suggests that the protonated form might initiate the catalytic reaction in comparison to the nonprotonated form, as reported earlier on model complexes.[23]

Because of the subtle energy differences among the peroxo- and hydroperoxodiiron(III/III) models, the structures and energetics computed alone are not sufficient to affirm the ground-state structure of the oxygen adduct of the AurF enzyme. In this situation, the energetics−spectroscopic approach, where the energetics and spectral parameters are computed side-by-side, provide further clues to narrow down the target.[5,8] Here we have adopted this approach and computed the MB parameters of all of the models and the UV−vis spectra of energetically low-lying models. In all of the computed model complexes, an AF interaction between the metal ions has been noted, leading to stabilization of the singlet ground state (see Figure 2). A net spin density of 3.8−4.0 (Table 1) indicates high-spin Fe^{III} centers. Inspection of the spin densities among the peroxo models reveals that, in models $_{227}$M3 and $_{227}$M3P, electron delocalization is significant in one of the bridging O atoms compared to the other. This suggests the presence of a radical character at this O center.

Also, the spin densities of the M1 and $_{227}$M1 models indicate the symmetric binding of the peroxo moiety to both Fe centers.[3h] The magnetic exchange interaction (J) is an extremely sensitive parameter to small structural changes, and this interaction is found to be AF in nature in all of the cases studied. Because there are significant structural changes, the computed J values also vary grossly across the series (see Tables 1 and S6). The computed J value of the models are in the range of −30.3 to −172.5 cm^{-1}, and this is in good accordance with the earlier reported values for the MMO model complex (−33 cm^{-1}).[24]

Although the general practice is to employ the electronic energy to compute the J values,[18b,25] here we have employed free energies because the molecular structures of the models studied are drastically different. In this case, the addition of free energy corrections to the total energy becomes important in the evaluation of the exchange constants. Although the magnitude of computed J using free and electronic energies varies, the trend of protonated models possessing less AF contribution to the J value is reflected in both sets (see Table S6). For the M2 model, the O atoms are found to gain significant spin densities, particularly on the distal O atom (see Figure 2). Because of the radical nature of the bridging group, there are three different exchange interactions, J_1−J_3, as defined in Figure 2b, and these are estimated to be −4.6, −119.5, and −365.5 cm^{-1}, respectively (see the Supporting Information for further details).[18c,d]

Table 1 shows the computed isomer shift (δ, IS) and quadruple splitting (ΔE_q, QS) parameters of all of the model complexes along with the experimental values. The observance of two different IS and QS values suggests that the enzyme has two Fe centers with different coordinating environments (asymmetric Fe sites). All of the peroxo models (the M1−M3 variations) have the δ values in the range of 0.65−0.75 mm/s. Similarly, for all hydroperoxo models, the δ value is in the range of 0.55−0.73 mm/s. Quite interestingly, the δ values observed experimentally are closer to the computed values of all models (especially M2P and $_{227}$M2P). However, a large deviation in the QS has been observed for all models except the M2P and $_{227}$M2P models (see Table 1).

The time-dependent DFT (TD-DFT)-computed spectrum for the $_{227}$M2P model (see Figure 3) shows a broad peak

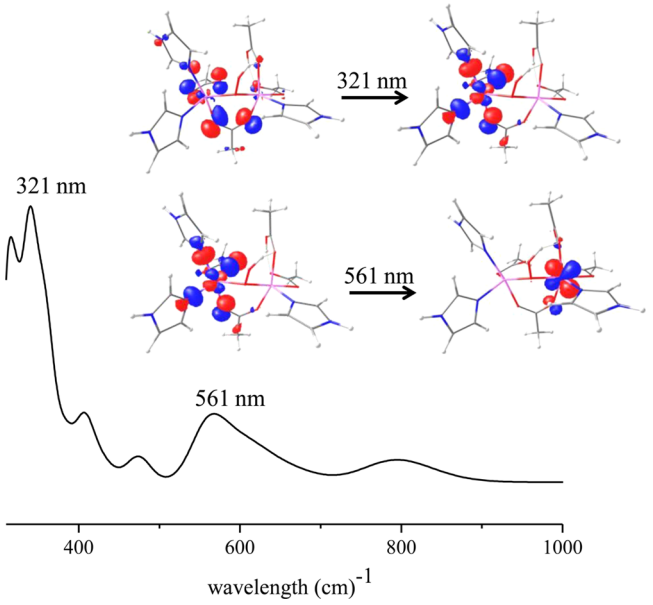

Figure 3. TD-DFT-calculated UV absorption of the model $_{227}$M2P. A contour plot of the orbitals corresponding to the excitation with maximum oscillator strength is shown. See ref 5 for experimental values.

around 561 nm and a sharp peak around 321 nm. This suggests ligand-to-metal charge-transfer excitation and is consistent with the experimental signal observed around 500 nm.[4b] Besides, we have also observed a weak charge-transfer transition at 406 nm. The spectral features resemble the spectra reported for the oxyhemerythrin enzyme possessing a μ-1,1-coordinated hydroperoxo active site, offering confidence on the computed data.[26] For the energetically close-lying M1P model, no transition around 500 nm was detected (see Figure 4). This suggests that

DOI: 10.1021/acs.inorgchem.5b00872
Inorg. Chem. 2015, 54, 11077−11082

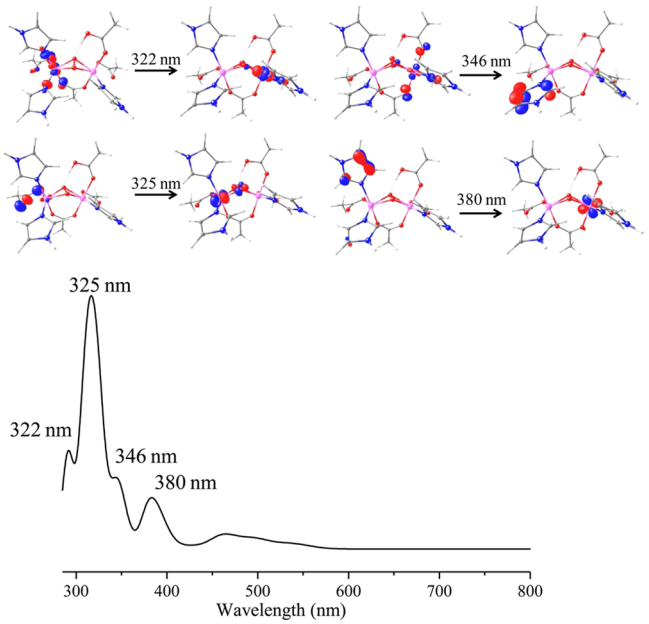

Figure 4. TD-DFT-calculated UV absorption of the model M1P. A contour plot of the orbitals corresponding to the excitation with maximum oscillator strength is shown. See ref 5 for experimental values.

the M1P model is unlikely to be the structure spectroscopically observed at the experimental conditions. Thus, by comparing the structure, energetics, and spectral features, we affirm here that the $_{227}$M2P model with μ-1,1-O_2 coordination is the most possible active site structure in the oxidized form of the enzyme ([(His)$_2$(Glu)Fe^{III}(μ-1,1-OOH)(μ-Glu)Fe^{III}(His)(Glu)(Glu-H)]). The Eigen value plot for the $_{227}$M2P model (see Figure 5) reflects the asymmetric nature of the Fe sites, where a significant overlap between the Fe(d_{xz}) and $\pi^*(O_2)$ orbitals is detected. Besides, because the Fe1 center has only five coordination, the orbital splitting and the order are also markedly different compared to the six-coordinate Fe2 center.

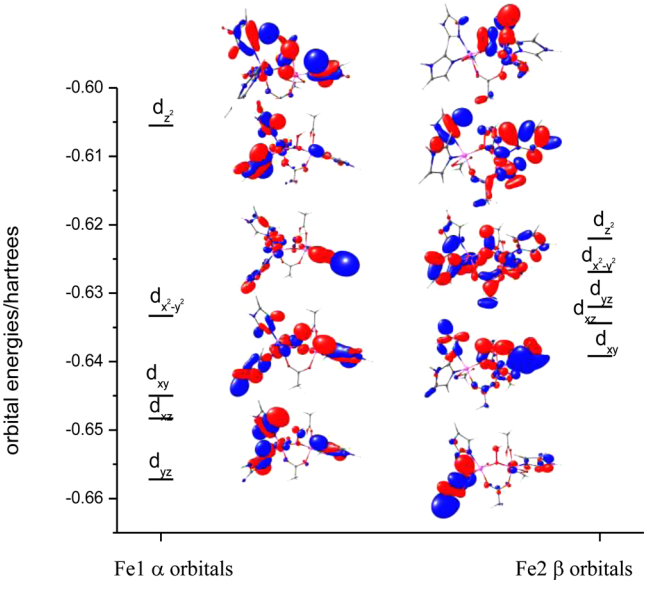

Figure 5. Energies and the counterplot of the Fe$^{III}O_2$-based orbitals of the $_{227}$M2P model.

DISCUSSION

From the structural parameters (see Figure 1 and Tablea S1 and S2), energetics (Table1), and NSP, first we tried to identify the ground-state structure of the oxygenated form of the diiron AurF. From Table 1, we found that, among the μ-1,1-coordinated hydroperoxo models, model M2P without glutamate protonation is 84.4 kJ/mol higher in energy than the $_{227}$M2P model. Also, we infer that its peroxo counterpart $_{227}$M2 is ∼43 kJ/mol higher in energy than the $_{227}$M2P model. From the calculated MB spectral parameters, we found that the overall δ values of all of the models compare closely with the observed experimental values (especially M2P and $_{227}$M2P). However, a large deviation in the QS parameters has been observed for all models except the M2P and $_{227}$M2P models. Considering the fact that M2P is higher in energy than $_{227}$M2P and the structural parameters of the latter is in good accordance with the X-ray structure, we propose the $_{227}$M2P model as the ground-state structure of the peroxo intermediate observed for the AurF enzyme.

Our computational investigation plays a vital role in strongly supporting the fact that, in the oxygenated Fe$^{III}_2$ site of the AurF enzyme, the O atom is present in the μ-1,1-coordination mode and both the peroxide and terminal glutamate residues are protonated. Comparing the QS value between the peroxo (1.22−0.95: $_{227}$M2) and hydroperoxo (−0.78, +0.78: $_{227}$M2P) models against the experimental values, we infer that $_{227}$M2P is comparable to the experimental data. Also, the TD-DFT-computed UV−vis data for the $_{227}$M2P model is also in agreement with the experimental observation. Thus, our results provide strong support for the ^{227}M2P structure as the possible active site structure of the oxygenated form of AurF, and this proposal supports the earlier experimental observations.[27]

CONCLUSIONS

In this work, we have studied 12 model complexes of the oxygenated Fe$^{III}_2$ site of the AurF enzyme to categorically assign the ground-state structure based on the energetics−spectroscopic approach whereby the energies and spectral parameters are calculated side-by-side. Our calculations incorporating several possible binding modes of O_2 and protonation sites reveal the $_{227}$M2P model, where O_2 is coordinated in a μ-1,1 fashion with the molecular formula of [(His)$_2$(Glu)Fe^{III}(μ-1,1-OOH)(μ-Glu)Fe^{III}(His)(Glu)(Glu-H)] as the ground-state structure of the oxygenated species. Efforts are underway now in our laboratory to understand the catalytic conversion of *p*-aminobenzoate to *p*-nitrobenzoate ($ArNO_2$) by this oxygenated species, and this will be reported in due course.

ASSOCIATED CONTENT

Supporting Information

The Supporting Information is available free of charge on the ACS Publications website at DOI: 10.1021/acs.inorgchem.5b00872.

Structural parameters, NSP, MB parameters, magnetic exchange coupling of the models investigated with B3LYP-D2 and B3LYP functionals, and the computed UV spectrum (PDF)

DOI: 10.1021/acs.inorgchem.5b00872
Inorg. Chem. 2015, 54, 11077−11082

AUTHOR INFORMATION

Corresponding Authors

*E-mail: prabha.jaypal@gmail.com. Tel: +91-22-2576-7183. Fax: +91-22-2572-3480.

*E-mail: rajaraman@gmail.com. Tel: +91-22-2576-7183. Fax: +91-22-2572-3480.

Notes

The authors declare no competing financial interest.

ACKNOWLEDGMENTS

P.J. thanks DST-India for the Fast Track young scientist fellowship (Grant SR/FT/CS-56-2011). A.A. thanks CSIR for a SRF fellowship. G.R. acknowledges the DST (Grant EMR/2014/000247) and DST Nanomission for funding.

REFERENCES

(1) Krebs, C.; Matthews, M. L.; Jiang, W.; Bollinger, J. M., Jr. *Biochemistry* **2007**, *46*, 10413−10418.

(2) Zocher, G.; Winkler, R.; Hertweck, C.; Schulz, G. E. *J. Mol. Biol.* **2007**, *373*, 65−74.

(3) (a) Stoian, S. A.; Xue, G.; Bominaar, E. L.; Que, L., Jr.; Munck, E. *J. Am. Chem. Soc.* **2014**, *136*, 1545−1558. (b) Sankaralingam, M.; Palaniandavar, M. *Polyhedron* **2014**, *67*, 171−180. (c) Han, W.; Liu, T.; Lovell, T.; Noodleman, L. *J. Am. Chem. Soc.* **2005**, *127*, 15778−15790. (d) Coggins, M. K.; Toledo, S.; Kovacs, J. A. *Inorg. Chem.* **2013**, *52*, 13325−13331. (e) Elango, N.; Radhakrishnan, R.; Froland, W.; Wallar, B.; Earhart, C.; Lipscomb, J.; Ohlendorf, D. *Protein Sci.* **1997**, *6*, 556−568. (f) Rosenzweig, A.; Nordlund, P.; Takahara, P.; Frederick, C.; Lippard, S. *Chem. Biol.* **1995**, *2*, 409−418. (g) Lindqvist, Y.; Huang, W.; Schneider, G.; Shanklin, J. *EMBO J.* **1996**, *15*, 4081−4092. (h) Skulan, A. J.; Brunold, T. C.; Baldwin, J.; Saleh, L.; Bollinger, J. M., Jr.; Solomon, E. I. *J. Am. Chem. Soc.* **2004**, *126*, 8842−8855.

(4) (a) Choi, Y. S.; Zhang, H.; Brunzelle, J. S.; Nair, S. K.; Zhao, H. *Proc. Natl. Acad. Sci. U. S. A.* **2008**, *105*, 6858−6863. (b) Korboukh, V. k.; Li, N.; Barr, E. W.; Bollinger, J. M., Jr.; Krebs, C. *J. Am. Chem. Soc.* **2009**, *131*, 13608−13609.

(5) Jayapal, P.; Rajaraman, G. *Phys. Chem. Chem. Phys.* **2012**, *14*, 9050−9053.

(6) Li, N.; Korboukh, V. K.; Krebs, C.; Bollinger, J. M., Jr. *Proc. Natl. Acad. Sci. U. S. A.* **2010**, *107*, 15722−15727.

(7) (a) Greco, C. *Dalton Trans.* **2013**, *42*, 13845−13854. (b) Saito, T.; Shoji, M.; Kanda, K.; Isobe, H.; Yamanaka, S.; Kitagawa, Y.; Yamada, S.; Kawakami, T.; Okumura, M.; Yamaguchi, K. *Int. J. Quantum Chem.* **2012**, *112*, 121−135. (c) Siegbahn, P. E. M.; Blomberg, M. R. A. *Chem. Rev.* **2010**, *110*, 7040−7061. (d) Ye, S.; Neese, F. *Curr. Opin. Chem. Biol.* **2009**, *13*, 89−98. (e) Pantazis, D. A.; Orio, M.; Petrenko, T.; Zein, S.; Bill, E.; Lubitz, W.; Messinger, J.; Neese, F. *Chem. - Eur. J.* **2009**, *15*, 5108−5123. (f) Rhee, Y. M.; Head-Gordon, M. *J. Am. Chem. Soc.* **2008**, *130*, 3878−3887.

(8) (a) Blomberg, M. R. A.; Siegbahn, P. E. M. *J. Comput. Chem.* **2006**, *27*, 1373−1384. (b) Neese, F. *Curr. Opin. Chem. Biol.* **2003**, *7*, 125−135. (c) Grimme, S. *J. Comput. Chem.* **2006**, *27*, 1787−1799.

(9) (a) Becke, A. D. *J. Chem. Phys.* **1993**, *98*, 5648−5652. (b) Becke, A. D. *Phys. Rev. A: At., Mol., Opt. Phys.* **1988**, *38*, 3098−3100. (c) Grimme, S. *J. Comput. Chem.* **2006**, *27*, 1787−1799.

(10) Schaefer, A.; Horn, H.; Ahlrichs, R. *J. Chem. Phys.* **1992**, *97*, 2571−2577. (b) Schaefer, C.; Huber, C.; Ahlrichs, R. *J. Chem. Phys.* **1994**, *100*, 5829−2835.

(11) Frisch, M. J.; Trucks, G. W.; Schlegel, H. B.; Scuseria, G. E.; Robb, M. A.; Cheeseman, J. R.; Scalmani, G.; Barone, V.; Mennucci, B.; Petersson, G. A.; Nakatsuji, H.; Caricato, M.; Li, X.; Hratchian, H. P.; Izmaylov, A. F.; Bloino, J.; Zheng,G.; Sonnenberg, J. L.; Hada, M.; Zhara, M.; Toyota,K.; Fukuda, R.; Hasegawa, J.; Ishida, M.; Nakajima, T.; Honda, Y.; Kitao, O.; Nakai, H.; Vreven, T.; Montgomery, J. A., Jr.; Peralta, J. E.; Ogliaro, F.; Bearpark, M.; Heyd, J. J.; Brothers, E.; Kudin, K. N.; Staroverov, V. N.; Kobayashi, R.; Normand, J.; Raghavachari, K.; Rendell, A.; Burant, J. C.; Iyengar, S. S.; Tomasi, J.; Cossi, M.; Rega, N.; Millam, J. M.; Klene, M.; Knox, J. E.; Cross, J. B.; Bakken, V.; Adamo, C.; Jaramillo, J.; Gomperts, R.; Stratmann, R. E.; Yazyev, O.; Austin, A. J.; Cammi, R.; Pomelli,C.; Ochterski, J. W.; Martin, R. L.; Morokuma, K.; Zakrzewski, V. G.; Voth, G. A.; Salvador, P.; Dannenberg, J. J.; Dapprich, S.; Daniels, A. D.; Farkas, Ö.; Foresman, J. B.; Ortiz, J. V.; Cioslowski, J.; Fox, D. J. *Gaussian 09*; Gaussian, Inc.: Wallingford, CT, 2009.

(12) (a) Neese, F. *Comput. Mol. Sci.* **2012**, *2*, 73−78. (b) Neese, F. *Density Functional and Semiempirical Program Package, version 2.8*; University of Bonn: Bonn, Germany, 2009.

(13) Römelt, M.; Ye, S.; Neese, F. *Inorg. Chem.* **2009**, *48*, 784−785. (b) Gasiorski, P.; Danel, K. S.; Matusiewicz, M.; Uchacz, T.; Kuźnik, W.; Piatek, L.; Kityk, A. V. *Mater. Chem. Phys.* **2012**, *132*, 330−338.

(14) (a) Ansari, A.; Kaushik, A.; Rajaraman, G. *J. Am. Chem. Soc.* **2013**, *135*, 4235−4249. (b) Ansari, A.; Rajaraman, G. *Phys. Chem. Chem. Phys.* **2014**, *16*, 14601−14613. (c) Pandey, B.; Ansari, A.; Vyas, N.; Rajaraman, G. *J. Chem. Sci.* **2015**, *127*, 343−352. (d) Ansari, M.; Vyas, N.; Ansari, A.; Rajaraman, G. *Dalton Trans.* **2015**, *44*, 15232−15243.

(15) Perdew, J. P. *Phys. Rev. B: Condens. Matter Mater. Phys.* **1986**, *33*, 8822−8824.

(16) Noodleman, L. *J. Chem. Phys.* **1981**, *74*, 5737−5743.

(17) (a) Ruiz, E.; Alvarez, S.; Rodriguez-Fortea, A.; Alemany, P.; Pouillon, Y.; Massobiro, C. In *Magnetism: Molecules to Materials II: Models and Experiments*; Miller, J. S., Drillon, M., Eds.; Wiley-VCH Verlag GmbH & Co. KGaA: New York, 2001; pp 227−279. (b) Bencini, A.; Totti, F.; Daul, C. A.; Doclo, K.; Fantucci, P.; Barone, V. *Inorg. Chem.* **1997**, *36*, 5022−5030.

(18) (a) Rajaraman, G.; Cano, J.; Brechin, K. E.; McInnes, E. J. L. *Chem. Commun.* **2004**, 1476−1477. (b) Berg, N.; Rajeshkumar, T.; Taylor, S. M.; Brechin, K. E.; Rajaraman, G.; Jones, L. F. *Chem. - Eur. J.* **2012**, *18*, 5906−5918. (c) Tewary, S.; Gass, I. A.; Murray, K. S.; Rajaraman, G. *Eur. J. Inorg. Chem.* **2013**, *2013*, 1024−1032. (d) Ansari, A.; Jayapal, P.; Rajaraman, G. *Angew. Chem., Int. Ed.* **2014**, *54*, 564−568.

(19) Note that the subscript 227 in front of M denotes its site 2 terminal glutamate being protonated; e.g., model $_{227}$M1 denotes model M1 with protonation at the Glu-227 residue. See also: Comba, P.; Rajaraman, G.; Rohwer, H. *Inorg. Chem.* **2007**, *46*, 3826−3838.

(20) (a) Gherman, B. F.; Baik, M. H.; Lippard, S. J.; Friesner, R. A. *J. Am. Chem. Soc.* **2004**, *126*, 2978−2990. (b) Rinaldo, D.; Philipp, D. M.; Lippard, S. J.; Friesner, R. J. *J. Am. Chem. Soc.* **2007**, *129*, 3135−3147. (c) Jayapal, P.; Sundararajan, M.; Hillier, I. H.; Burton, N. A. *Phys. Chem. Chem. Phys.* **2006**, *8*, 4086−4094.

(21) (a) Sazinsky, M. H.; Bard, J.; Di Donato, A.; Lippard, S. J. *J. Biol. Chem.* **2004**, *279*, 30600−30610. (b) Murray, L. J.; Garcia-Serres, R.; McCormick, M. S.; Davydov, R.; Naik, S. G.; Kim, S. H.; Hoffman, B. M.; Huynh, B. H.; Lippard, S. J. *Biochemistry* **2007**, *46*, 14795−14809.

(22) Bochevarov, A. D.; Li, J.; Song, W. J.; Friesner, R. A.; Lippard, S. J. *J. Am. Chem. Soc.* **2011**, *133*, 7384−7397.

(23) (a) McClune, G. J.; Fee, J. A.; McCluskey, G. A.; Groves, J. T. *J. Am. Chem. Soc.* **1977**, *99*, 5220−5222. (b) Walling, C.; Kurz, M.; Schugar, H. J. *Inorg. Chem.* **1970**, *9*, 931−937. (c) Thewalt, U.; Marsh, R. *J. Am. Chem. Soc.* **1967**, *89*, 6364−6365.

(24) Brunold, T. C.; Tamura, N.; Kitajima, N.; Moro-Oka, Y.; Solomon, E. I. *J. Am. Chem. Soc.* **1998**, *120*, 5674−5690.

(25) (a) Singh, S. K.; Tibrewal, N. K.; Rajaraman, G. *Dalton Trans.* **2011**, *40*, 10897−10906. (b) Rajaraman, G.; Totti, F.; Bencini, A.; Caneschi, A.; Sessoli, R.; Gatteschi, D. *Dalton Trans.* **2009**, 3153−3161. (c) Gupta, T.; Rajeshkumar, T.; Rajaraman, G. *Phys. Chem. Chem. Phys.* **2014**, *16*, 14568−14577.

(26) (a) Stenkamp, R. E. *Chem. Rev. (Washington, DC, U. S.)* **1994**, *94*, 715−726. (b) Shiemke, A. K.; Loehr, T. M.; Sanders-Loehr, J. *J. Am. Chem. Soc.* **1986**, *108*, 2437−2443.

(27) Chanco, E.; Choi, Y. S.; Sun, N.; Vu, M.; Zhao, H. *Bioorg. Med. Chem.* **2014**, *22*, 5569−5577.

DOI: 10.1021/acs.inorgchem.5b00872
Inorg. Chem. 2015, 54, 11077−11082